Separation Science and Technology
Publication details, including instructions for authors and subscription information:
http://www.informaworld.com/smpp/title~content=t713708471

Time-Dependent Foam Flotation Stripping Column Operation

Judy E. Kiefer[a]; David J. Wilson[a]
[a] DEPARTMENT OF CHEMISTRY, VANDERBILT UNIVERSITY, NASHVILLE, TENNESSEE

To cite this Article Kiefer, Judy E. and Wilson, David J.(1981) 'Time-Dependent Foam Flotation Stripping Column Operation', Separation Science and Technology, 16: 2, 147 — 171
To link to this Article: DOI: 10.1080/01496398108058110
URL: http://dx.doi.org/10.1080/01496398108058110

SEPARATION SCIENCE AND TECHNOLOGY, 16(2), pp. 147–171, 1981

Time-Dependent Foam Flotation Stripping Column Operation

JUDY E. KIEFER and DAVID J. WILSON*

DEPARTMENT OF CHEMISTRY
VANDERBILT UNIVERSITY
NASHVILLE, TENNESSEE 37235

Abstract

A mathematical model for the time-dependent operation of a foam flotation stripping column is presented. Solute and solvent balances are developed for the stripping and foam drainage sections of the column, and a Langmuir isotherm is assumed for the surface-active solute. Results of computations with the model illustrate the dependence of column performance on influent and air flow rates, pulse hydraulic and solute concentrations, bubble size, and column geometry. Boundary layer theory is used to calculate the efficiency of foam flotation from a pool of liquid as a function of bubble size.

INTRODUCTION

Adsorptive bubble separation techniques are of some interest for the removal of small amounts of heavy metals and other toxic substances from aqueous solution. These methods have been reviewed by Lemlich (*1*) and others (*2–4*, for example). Several mathematical models for foam column operation have been published; these are generally obtained from steady-state material balance considerations at the ends of the column (*1*, *5*, *6*). Goldberg and Rubin discussed these models in some detail, and analyzed a model of a stripping column without solute transfer in the countercurrent section (*7*). Wang's treatment of continuous bubble fractionation includes axial dispersion and equilibrium adsorption isotherms (*8*). Cannon and Lemlich presented a detailed analysis assuming linear isotherms (*9*), as has Lee (*10*). Fanlo and Lemlich (*11*); Grieves, Bhattacharyya, and their co-workers (*12*); Valdes-Krieg, King, and

*To whom correspondence should be addressed.

Sephton (*13*); and Sastry and Fuerstenau (*14*) have also examined the modeling of flotation column operation.

We earlier analyzed a continuous flow foam flotation column operating at steady state in the stripping mode (*15*). The model included effects of axial dispersion, rate of mass transfer, and nonlinear isotherms. It did not, however, provide a way of calculating the wetness of the foam. Also, in actual practice such columns are generally not operated in the steady state; in wastewater treatment it is almost the rule that influent flow rate and solute concentrations vary considerably with time. In order to predict the effects of such variations, a time-dependent model is needed. This would permit estimation of the solute removal efficiency of a column under intermittent shock hydraulic and concentration loadings.

Here we develop a model for the time-dependent operation of a continuous-flow foam flotation column consisting of a stripping section and a foam drainage section. We use Haas and Johnson's analysis of foam drainage (*6*) and detailed material balances throughout the column. The resulting differential equations are integrated forward in time by means of a predictor-corrector method. We then give a discussion of some of the numerical results obtained. We close with an application of boundary layer theory to the calculation of the efficiency of particle flotation by bubbles rising through a pool of liquid.

ANALYSIS

We first address the problem of foam drainage. The foam is assumed to consist of bubbles in the shape of regular dodecahedra, as is generally assumed in fairly dry foams (*6*, *16*). Recall that a dodecahedron is a regular polyhedron with 12 regular pentagonal faces and 30 edges. If we let l be the length of one of these edges, then the surface area of the dodecahedron is $20.64578l^2$, and its volume is $7.66312l^3$ (*17*). We also assume that all the bubbles are of identical size, with a volume equal to the volume of a sphere of diameter d.

In following the analysis of Haas and Johnson (*16*), we assume that the Plateau borders formed by three adjacent bubbles can be approximated as capillaries of diameter δ, where δ depends on the wetness of the foam. The liquid in these capillaries flows downward due to gravitational forces; the flow can be described by Poiseuille's equation

$$v = \frac{\Delta P \delta^2}{32\eta l} \tag{1}$$

where v = velocity of the liquid relative to the capillary
η = liquid viscosity, poise

l = capillary length
ΔP = pressure drop along the length of the capillary

The pressure drop due to the hydrostatic head in the capillary is given by

$$\Delta P = \rho g l \cos\theta \tag{2}$$

where ρ = liquid density
g = gravitational constant
θ = angle at which capillary is inclined from the vertical

With this result, Eq. (1) becomes

$$v = \frac{\rho g \cos\theta \delta^2}{32\eta} \tag{3}$$

the velocity for liquid in a capillary inclined at an angle θ from the vertical. The component of this velocity in the downward direction, v_z, is $v \cos\theta$. The average velocity of the liquid in the z-direction (downward) relative to the rising foam, $\bar{v}_z$, is then given by

$$\begin{aligned}\bar{v}_z &= \frac{\int_0^{\pi/2} v_z \sin\theta \, d\theta}{\int_0^{\pi/2} \sin\theta \, d\theta} \\ &= \frac{\rho g \delta^2}{32\eta} \frac{\int_0^{\pi/2} \cos^2\theta \sin\theta \, d\theta}{\int_0^{\pi/2} \sin\theta \, d\theta} \\ &= \frac{1}{3}\frac{\rho g \delta^2}{32\eta}\end{aligned} \tag{4}$$

Since the foam is moving upward at a velocity v_s, the downward velocity relative to the laboratory of the liquid in the Plateau borders is

$$v_{\text{lab}} = \bar{v}_z - v_s \tag{5}$$

We define ε_{PB} as the volume of liquid in the Plateau borders per unit volume of foam. This is also the area available for liquid flow downward per unit area of column cross section. The liquid flux ($cm^3/cm^2 s$) through the Plateau borders relative to the lab is therefore

$$F = (\bar{v}_z - v_s)\varepsilon_{PB} \tag{6}$$

Liquid is also contained in the thin films (lamellae) which are the boundary surfaces of the dodecahedra, so we write

$$\varepsilon_{PB} + \varepsilon_f = \varepsilon \tag{7}$$

where ε = volume of liquid per unit volume of foam
ε_f = volume of liquid in lamellae per unit volume of foam

Haas and Johnson make the assumption that the Plateau borders contain two-thirds of the liquid in the foam; we leave this fraction as an adjustable parameter, β.

There are $6(1 - \varepsilon)/\pi d^3$ bubbles per unit volume of foam, 10 Plateau borders per dodecahedral bubble (30 edges per dodecahedron, with three edges of adjacent dodecahedra meeting to form a border), and each Plateau border has a volume of $\pi\delta^2 l/4$, where l is the length of an edge of a dodecahedron. This yields

$$\varepsilon_{PB} = \frac{6(1 - \varepsilon)}{\pi d^3} 10 \frac{\pi\delta^2 l}{4} \tag{8}$$

Since $l = 0.4088d$ and we are assuming that

$$\varepsilon_{PB} = \beta\varepsilon \tag{9}$$

we obtain

$$\varepsilon_{PB} = 6.132 \frac{(1 - \varepsilon)\delta^2}{d^2} \tag{10}$$

and

$$\delta^2 = 0.1631 \frac{\beta\varepsilon d^2}{1 - \varepsilon} \tag{11}$$

The velocity of the bubble surfaces upward is given by

$$v_s = \frac{G}{A(1 - \varepsilon)} \tag{12}$$

where G = gas flow rate, mL/s
A = column cross section, cm^2

Combining Eqs. (4), (6), (9), (11), and (12) results in an expression for F, the liquid flux downward through the Plateau borders, as a function of ε, d, β, and other known quantities:

$$F = 1.699 \times 10^{-3} \frac{\rho g d^2}{\eta} \frac{\beta^2\varepsilon^2}{1 - \varepsilon} - \frac{G\beta\varepsilon}{A(1 - \varepsilon)} \tag{13}$$

The bubble diameter d can be determined experimentally for various gas

dispersion heads. Lemlich (*18*) has noted that for a distribution of bubble sizes, d^2 should be calculated as

$$d^2 = \sum n_i d_i^3 / \sum n_i d_i$$

ρ, η, G, and A are also known, and ε is calculated as a function of time and position by means of solvent balances, as shown below. This leaves β as the only adjustable parameter.

In our model we require an expression for the surface area per unit volume of foam, S. The surface area of a dodecahedron is $3.4506d^2$ (*17*), which yields for the surface area per unit volume of bubbles

$$\frac{3.4506d^2}{\pi d^3/6} = \frac{6.59}{d}$$

and then

$$S = \frac{6.59}{d}(1 - \varepsilon) \tag{14}$$

Equations (12), (13), and (14) will be used in the material balance equations below to express derivatives in terms of known properties, β, ε, and solute concentration c, where ε and c are function of time and position in the column.

In foam flotation the solute to be removed is (or is made) surface active so that it will adsorb to the surface of a rising bubble and be removed in the foam. Huang (*19*) and Kennedy (*20*) have shown that the surface concentration of a surface-active solute of floc reaches its local equilibrium concentration quite quickly under these conditions—the decay constant for the approach to equilibrium is the order of a microsecond. We can therefore safely assume that the surface concentration of solute is always in local equilibrium with the liquid concentration. We use a Langmuir adsorption isotherm

$$\Gamma = \frac{\Gamma_{max} c}{c_{1/2} + c} \tag{15}$$

where Γ = surface concentration, mol/cm^2
Γ_{max} = maximum possible surface concentration
$c_{1/2}$ = concentration of solute in liquid when $\Gamma = \frac{1}{2}\Gamma_{max}$
c = concentration of solute in liquid, mol/cm^2

The column is partitioned into N horizontal slabs of equal size, as shown in Fig. 1, so that we may carry out solute and solvent material balances. Each slab is considered to be completely mixed, and we assume

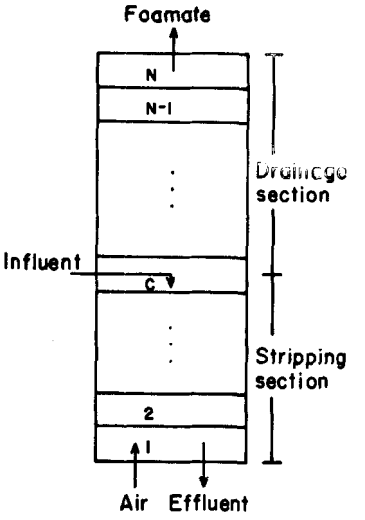

FIG. 1. The foam flotation column being modeled.

no mixing between adjacent slabs. Therefore, solvent flows into a slab through Plateau borders only from the slab above it if $F > 0$ and from the slab below it if $F < 0$; solvent also moves into the slab in the lamellae rising from the slab through the drainage of its own Plateau borders and from liquid in the lamellae of the bubbles leaving the slab. We also make a similar analysis of solute movement; here we must take into account transfer of solute between the liquid and surface phases.

In general, the solvent balance equations contain five terms, as described above,

$$\frac{d\varepsilon_n}{dt} = [F_{n+1}S'(F_{n+1}) - |F_n| - F_{n-1}S(-F_{n-1}) + v_{s,n-1}\varepsilon_{f,n-1} - v_{sn}\varepsilon_{f,n}]/\Delta x \tag{16}$$

where F_j = liquid flux through the Plateau borders in the jth slab; see Eq. (13)

$S'(z) = 1$ if $z > 0$

$= 0$ if $z \leq 0$

$v_{s,j}$ = foam velocity in slab j, given by Eq. (12)

ε_j = the value of ε in the jth slab

$\varepsilon_{f,j} = (1 - \beta)\varepsilon_j$, the volume fraction of liquid in the lamellar films in the jth slab

Δx = thickness of a slab

The slabs are numbered from the bottom of the column. The corresponding equations for the bottom and top slabs and the slab which receives the feed to the column require modification. The equation for the bottom slab does not contain the terms resulting from solvent entering from below; the equation for the top (Nth) slab does not contain the term resulting from solvent drainage from above. At the bottom

$$\frac{d\varepsilon_1}{dt} = [F_2 S'(F_2) - |F_1| - v_{s,1}\varepsilon_{f,1}]/\Delta x \tag{17}$$

At the top

$$\frac{d\varepsilon_N}{dt} = [-F_{N-1}S'(-F_{N-1}) - |F_N| + v_{s,N-1}\varepsilon_{f,N-1} - v_{s,N}\varepsilon_{f,N}]/\Delta x \tag{18}$$

At the slab containing the feed plane

$$\frac{d\varepsilon_c}{dt} = \left[\frac{Q}{A} F_{c+1}S'(F_{c+1}) - |F_c| - F_{c-1}S'(-F_{c-1}) + v_{s,c-1}\varepsilon_{f,c-1} - v_{s,c}\varepsilon_{f,c}\right]\Big/\Delta x \tag{19}$$

where Q = volumetric feed rate, mL/s.

A slightly different equation is used if the feed enters directly at the top of the column.

We let m_n be the mass of solute in slab n, and note that

$$m_n = (S_n\Gamma_n + \varepsilon_n c_n)A\Delta x \tag{20}$$

From Eq. (15)

$$\Gamma_n = \Gamma_{max}c_n/(c_{1/2} + c_n) \tag{21}$$

so

$$m_n = \left[\frac{S_n\Gamma_{max}c_n}{c_{1/2} + c_n} + \varepsilon_n c_n\right]A\Delta x \tag{22}$$

This can be written as a quadratic equation in c_n:

$$0 = \varepsilon_n A\Delta x c_n^2 + (S_n\Gamma_{max}A\Delta x + \varepsilon_n A\Delta x c_{1/2} - m_n)c_n - m_n c_{1/2} \tag{23}$$

which can be solved for c_n. Substitution in Eq. (21) then yields Γ_n.

Solute material balance on the nth slab then yields

$$\frac{dm_n}{dt} = A[S'(F_{n+1})F_{n+1}c_{n+1} - |F_n|c_n - S'(-F_{n-1})F_{n-1}c_{n-1} + v_{s,n-1}\varepsilon_{f,n-1}c_{n-1} - v_{s,n}\varepsilon_{f,n}c_n + v_{s,n-1}S_{n-1}\Gamma_{n-1} - v_{s,n}S_n\Gamma_n] \tag{24}$$

At the top of the column we have

$$\frac{dm_N}{dt} = A[-|F_N|c_N - S'(-F_{N-1})F_{N-1}c_{N-1} + v_{s,N-1}\varepsilon_{f,N-1}c_{N-1} - v_{s,N}\varepsilon_{f,N}c_N + v_{s,N-1}S_{N-1}\Gamma_{N-1} - v_{s,N}S_N\Gamma_N] \quad (25)$$

At the bottom of the column

$$\frac{dm_1}{dt} = A[S'(F_2)F_2c_2 - |F_1|c_1 - v_{s,1}\varepsilon_{f,1}c_1 - v_{s,1}S_1\Gamma_1] \quad (26)$$

At the feed plane

$$\frac{dm_c}{dt} = Qc^\circ + A[S'(F_{c+1})F_{c+1}c_{c+1} - |F_c|c_c - S'(-F_{c-1})F_{c-1}c_{c-1} + v_{s,c-1}\varepsilon_{f,c-1}c_{c-1} - v_{s,c}\varepsilon_{f,c}c_c + v_{s,c-1}S_{c-1}\Gamma_{c-1} - v_{s,c}S_c\Gamma_c] \quad (27)$$

We integrate Eqs. (16)–(19) and (24)–(27) forward in time using a simple predictor-corrector method having the following algorithm:

Starter:

$$y(\Delta t) = y(0) + \Delta t \frac{dy}{dt}(0) \quad (28)$$

Predictor:

$$y^*(t + \Delta t) = y(t - \Delta t) + 2\Delta t \frac{dy}{dt}(t) \quad (29)$$

Corrector:

$$y(t + \Delta t) = y(t) + \frac{\Delta t}{2}\left[\frac{dy}{dt}(t) + \frac{dy^*}{dt}(t + \Delta t)\right] \quad (30)$$

We next need to determine the amounts of solute and water leaving the top of the column as foamate and the bottom of the column as effluent. From Eq. (25) we can see that the mass of solute leaving the top of the column per second in the foamate is given by

$$M_{\text{foam}} = A[-S'(-F_N)F_Nc_N + v_{s,N}\varepsilon_{f,N}c_N + v_{s,N}S_N\Gamma_N] \quad (31)$$

The volume of liquid leaving the top of the column per second is

$$V_{\text{foam}} = A[-S'(-F_N)F_N + v_{s,N}\varepsilon_{f,N}] \quad (32)$$

The mass of solute leaving the bottom of the column per second is

$$M_{\text{effl}} = AS'(F_1)F_1c_1 \tag{33}$$

The volume of liquid leaving the bottom of the column per second is

$$V_{\text{effl}} = AS'(F_1)F_1 \tag{34}$$

The concentrations of the solute in the foamate and effluent are given by

$$c_{\text{foam}} = M_{\text{foam}}/V_{\text{foam}} \tag{35}$$

and

$$c_{\text{effl}} = M_{\text{effl}}/V_{\text{effl}} \tag{36}$$

Several parameters can be used to characterize the quality of the separation in various ways. One is the ratio of influent to effluent solute flux,

$$R_{\text{solute}} = Qc^\circ/M_{\text{effl}} \tag{37}$$

Another is the ratio of influent to foamate volumetric flow rates,

$$R_{\text{vol}} = Q/V_{\text{foam}} \tag{38}$$

A third is the ratio of influent to effluent solute concentrations,

$$R_{\text{conc}} = c^\circ/c_1 \tag{39}$$

RESULTS

The parameters generally used in the computer program simulating column operation are as follows:

column length	244 cm
column cross-sectional area	670 cm^2
number of slabs into which the column is partitioned	10
index of the feed plane slab	5
Γ_{max}	6×10^{-10} mol/cm^2
$c_{1/2}$	1×10^{-9} mol/cm^3
air flow rate	400 mL/s
liquid flow rate	150 mL/s
β	0.75
bubble diameter	0.25 cm
liquid density	1.0 g/mL
liquid viscosity	0.009 poise
influent concentration	1×10^{-8} mol/cm^3
Δt	0.1 s

The column parameters correspond to a small pilot-plant column we have operated. These parameters, an initial column solute concentration of 10^{-9} mol/mL, and a value of $\varepsilon = 0.10$ were used to initialize a run, which was then simulated for 30 min of column operation. The resulting state of the column was used as initial conditions for all of the runs described below. This initialization procedure markedly reduces the computer time required for the column to approach steady-state operation. All runs were made on a DEC system 1099 computer.

The effect of influent concentration on effluent concentration for various influent flow rates in steady-state operation is shown in Fig. 2. The Langmuir isotherm we are using gives us quite good removal efficiencies up almost to the point at which the bubbles are saturated, above which further increases in influent concentration result in a rather abrupt deterioration of removal efficiency. Figures 3a and 3b show the rate of approach to the new steady state when the influent concentration is changed abruptly at time zero. The transient responses of the column to square-wave shock influent concentration pulses of various heights and durations are exhibited in Figs. 4–6. The time constant of the system appears to be of the order of 5 min, and it is apparent that the column can absorb short concentration overloads without discharging effluent of the poor quality which one would expect on the basis of steady-state performance.

The effect of influent flow rate on steady-state effluent solute concentration is shown in Fig. 7 for various influent concentrations. As the influent solute flux increases with increasing flow rate, the column eventually

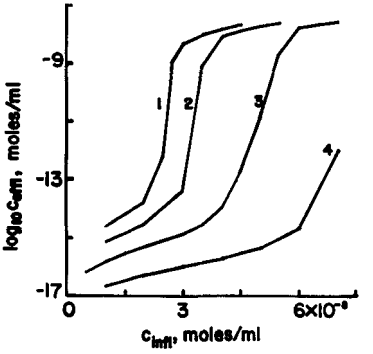

FIG. 2. Effluent concentration as a function of influent concentration at various flow rates in steady state operation. Influent flow rate = 250 (1), 200 (2), 150 (3), and 100 mL/s; other parameters as given in the text, as is the case through Fig. 15.

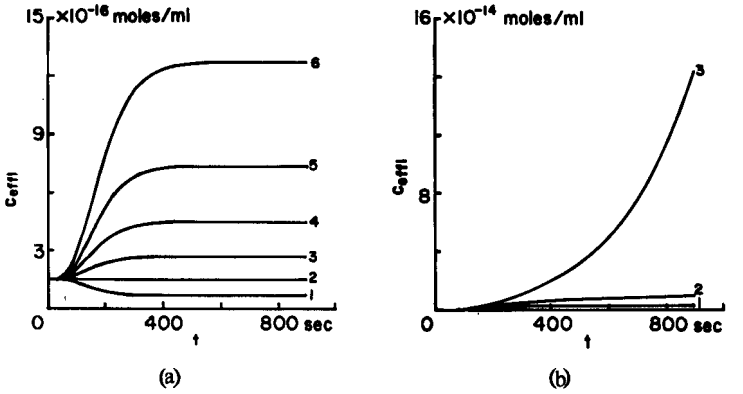

FIG. 3a. Effluent concentration as a function of time for influent concentrations of 0.5, 1.0, 1.5, 2.0, 2.5, and 3.0 $\times$ 10^{-8} mol/mL (1 through 6).
FIG. 3b. Effluent concentration as a function of time for influent concentrations of 3.5, 4.0, and 4.5 $\times$ 10^{-8} mol/mL (1 through 3).

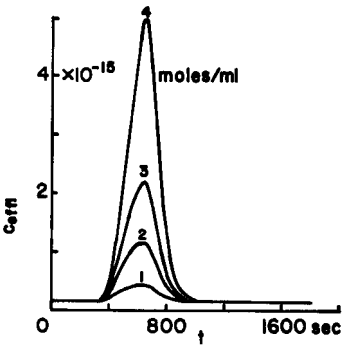

FIG. 4. Effluent concentration as a function of time for 5-min square-wave influent concentration pulses. The influent concentration is 1 $\times$ 10^{-8} mol/mL for $0 < t < 300$ s and for $t > 600$ s. For $300 < t < 600$ s, $c_{infl} = 2.0$ (1), 3.0 (2), 3.5 (3), and 5.0 (4) $\times$ 10^{-8} mol/mL.

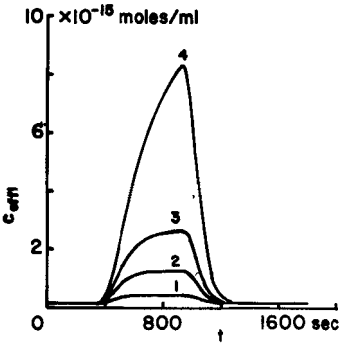

FIG. 5. Effluent concentration as a function of time for 10-min square-wave influent concentration pulses. The influent concentration is 1×10^{-8} mol/mL for $0 < t < 300$ s and $t > 900$ s. For $300 < t < 900$ s, $c_{infl} = 2.0$ (1), 3.0 (2), 3.5 (3), and 4.0 (4) $\times 10^{-8}$ mol/mL.

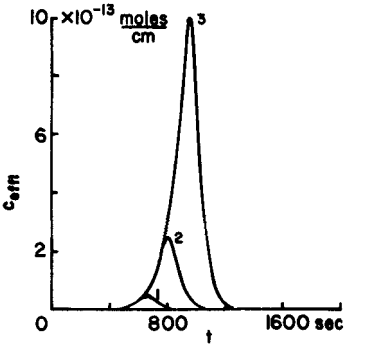

FIG. 6. Effluent concentration as a function of time for square-wave influent concentration pulses of various durations. $c_{infl} = 1 \times 10^{-8}$ mol/mL for $0 < t < 300$ s and for $\tau < t < 1800$ s. For $300 < t < \tau$, $c_{infl} = 5 \times 10^{-8}$ mol/mL. $\tau = 600$ (1), 750 (2), and 900 (3) s.

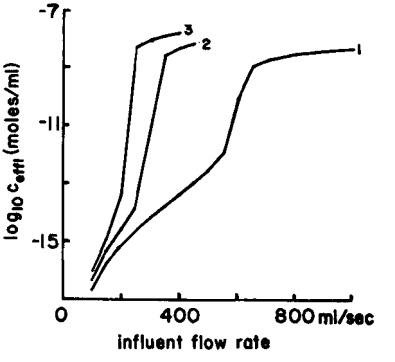

FIG. 7. Steady-state effluent concentration as a function of influent flow rate. $c_{infl} = 1.0$ (1), 2.0 (2), and 3.0 (3) $\times 10^{-8}$ mol/mL.

reaches the point where all the available air–water interface is saturated, at which point the effluent concentration abruptly increases. The effects of transient square-wave variations in the influent flow rate are shown in Fig. 8. These runs show that small flow rate increases of long duration result in less discharge of solute in the effluent than larger increase in flow rate for correspondingly shorter time periods. Evidently foam flotation columns should be used with flow equalization tanks if flow rate transients are expected.

Air–water interface is the "reagent" which brings about solute removal; if its availability is decreased by decreasing the air flow rate, one would expect the efficiency of solute removal from the effluent to decrease. In Fig. 9 we see that this is in fact the case, and that the column requires a

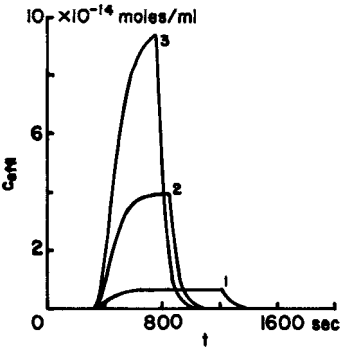

FIG. 8. Effluent concentration as a function of time for various square-wave influent flow rate pulses. The base influent flow rate is 150 mL/s. For Run 1 the influent flow rate for $300 < t < 1200$ s is 300; for Run 2, $300 < t < 840$ s, it is 400; for Run 3, $300 < t < 750$ s, it is 450 mL/s.

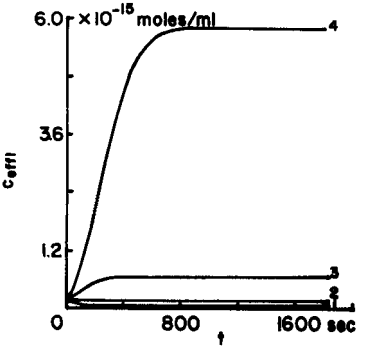

FIG. 9. Effluent concentration as a function of time for air flow rates of 500 (1), 500 (2), 300 (3), and 200 (4) mL/s.

few hundred seconds to approach a new steady state after an abrupt change in air flow rate at time zero. One obtains substantially lower effluent concentrations at increased air flow rates, but part of the price paid for this is an increased discharge of liquid in the foam, as seen in Fig. 10. We see a rather uneven approach to steady-state operation at the higher air flow rates here.

One of the column parameters which can readily be varied experimentally is the position of the influent feed. We next examine the effects on column performance that result from variations in the height of the influent feed. Figure 11 exhibits the effect of influent feed height on effluent solute concentration as a function of influent concentration. As expected, the more foam through which the influent must cascade before

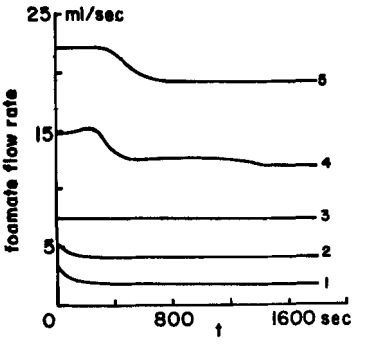

FIG. 10. Foamate volumetric flow rate as a function of time for air flow rates of 200 (1), 300 (2), 500 (3), 500 (4), and 600 (5) mL/s.

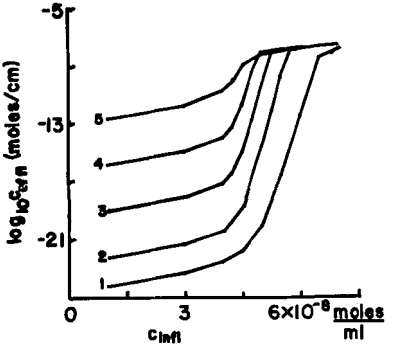

FIG. 11. Steady-state effluent concentration as a function of influent concentration for various feed heights. Index of slab containing the influent feed head = 10 (1), 9 (2), 7 (3), 5 (4), and 3 (5).

reaching the bottom of the column, the more complete the removal. Also, and this was unexpected, the greater the influent feed height, the higher the influent concentration required to produce extensive solute breakthrough in the effluent. Figure 12 shows plots of effluent concentration versus height of influent feed for a number of influent solute concentrations.

Increasing the height of the influent feed decreases the length of the foam drainage section of the flotation column, so that the flux of liquid in the foam discharged at the top of the column should increase. This is seen to be the case in Fig. 13. Under the conditions of these runs, however, a relatively short drainage section (feed plane index = 7, length

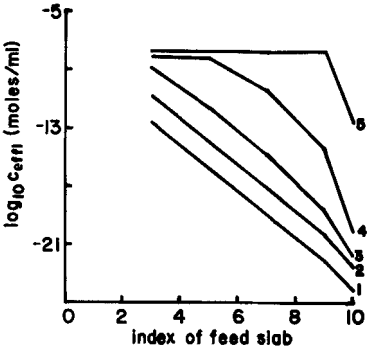

FIG. 12. Steady-state effluent concentration as a function of feed position for influent concentrations of 1.0 (1), 4.0 (2), 4.5 (3), 5.0 (4), and 6.0 (5) $\times 10^{-8}$ mol/mL.

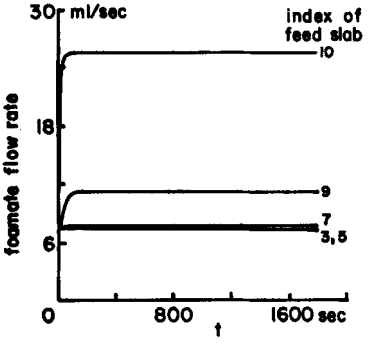

FIG. 13. Foamate flow rate as a function of time for feed slab indices of 3, 5, 7, 9, and 10.

of drainage section $\cong$ 85.4 cm) provides almost optimal drainage, so long drainage sections would appear to be unnecessary.

The flux of air–water interface decreases with increasing bubble size (other parameters held constant), so we expect increased bubble sizes to be associated with increased effluent solute concentration, as is shown to be the case in Fig. 14. Money spent on air dispersion heads which provide a foam of small bubbles without excessive pressure drop is evidently money well spent. We see in Fig. 15 that the effluent flow rate decreases slightly with decreasing bubble size, which is due to a wetter foam being discharged from the column as the bubbles are made smaller. Qualitatively, this is what one would expect.

This program permits us to conveniently model all aspects of the time-dependent operation of a continuous flow column with stripping and

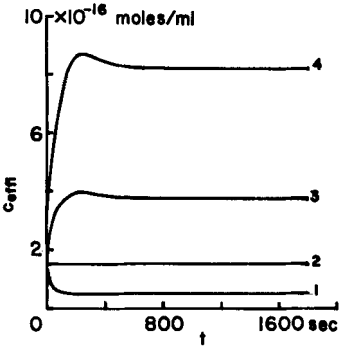

FIG. 14. Effluent concentration as a function of time for bubble diameters of 0.20 (1), 0.25 (2), 0.30 (3), and 0.35 (4) cm.

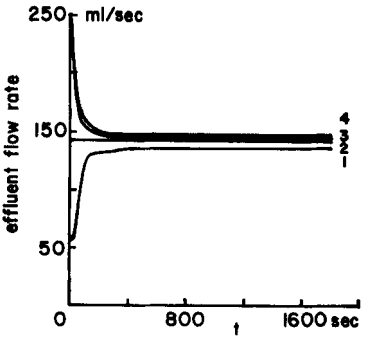

FIG. 15. Effluent flow rate as a function of time for bubble diameters of 0.20 (1), 0.25 (2), 0.30 (3), and 0.35 (4) cm.

drainage sections. Quite minor modifications in the program can be made to include the effects of effluent recycle and/or return of a fraction of the foamate for reflux.

PARTICLE DETACHMENT

It was shown earlier that thermal forces are extremely small compared to the viscous drag forces tending to detach floc particles from bubbles in the flotation of particulate material from a liquid pool (*21*, *22*). A rather detailed fluid mechanical calculation of the viscous drag forces on a particle attached to a rising bubble showed that tangential forces are much larger than radial forces (*23*), and suggested a "squeeze-out" model for particle detachment. In this model the floc particles occur in a "cap" on the bottom of the rising bubble; if viscous drag forces become too large, particles are squeezed out of the bottom of the cap until its size is reduced to the point where the tangential stress is no longer able to eject particles bound to the air–water interface. A simplified version of this model has been analyzed (*24*). In that calculation the viscous drag per unit area of bubble was taken as an average value, independent of position. In fact, the magnitude of the viscous drag varies a great deal over the surface of a rising bubble, and one must also take boundary layer separation into account for bubbles which are too large to be in the creeping flow regime. We do not wish the bubbles to be in the creeping flow regime, since this leads to quite small capture cross sections (*25*). We here give an analysis of the "squeeze-out" model which takes into account boundary layer separation and the variation of tangential stress with position, and is applicable to bubbles having large Reynolds numbers ($\leq 10^4$).

We assume that the streamlines and velocity of the fluid relative to the bubble some distance from the bubble are those which pertain in the inviscid flow regime, and that we must match boundary layer solutions to the inviscid solutions as is done by Schlichting (*26*). See Fig. 16. We calculate the rise velocity of the bubble, u_∞, from Ref. *27*:

$$u_\infty = \frac{2g\rho R^2}{9\eta\left[1 + \frac{1}{4}\left(\frac{\rho R u_\infty}{2\eta}\right)^{1/2} + \frac{0.34\rho R u_\infty}{12\eta}\right]} \tag{40}$$

This equation is valid for Reynolds numbers in the range

$$0 \leq \mathrm{Re} = \frac{2Ru_\infty\rho}{\eta} < 10^4 \tag{41}$$

Here g = gravitational constant

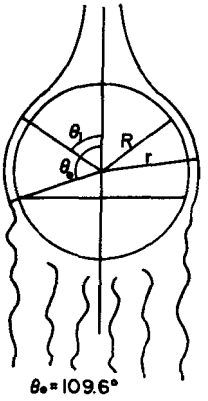

FIG. 16. Boundary layer separation in the inviscid flow regime. Notation.

ρ = fluid density
R = bubble radius
η = fluid viscosity (poise)

Bird, Stewart, and Lightfoot (*28*) give the stream function and velocity potential for inviscid ideal flow past a sphere; these are

$$\psi = \frac{u_\infty}{2}\left(\frac{R^3}{r} - r^2\right)\sin^2\theta \qquad \text{(stream function)} \tag{42}$$

$$\psi = u_\infty\left(\frac{R^3}{2r^2} + r\right)\cos\theta \qquad \text{(velocity potential)} \tag{43}$$

The velocity components (relative to the bubble) for inviscid ideal flow in this case are

$$U_r = -\frac{\partial\phi}{\partial r} = -u_\infty\left(-\frac{R^3}{r^3} + 1\right)\cos\theta \tag{44}$$

and

$$U_\theta = -\frac{1}{r}\frac{\partial\phi}{\partial\theta} = u_\infty\left(\frac{R^3}{2r^3} + 1\right)\sin\theta \tag{45}$$

Here r and θ are spherical coordinates with the polar axis in the direction of motion of the bubble. In the boundary layer adjacent to the bubble the velocity departs from the inviscid ideal case; we denote the velocity components in the boundary layer by u_r and u_θ. In the boundary layer we must have $u_r = 0$, and we see that $U_r(r \to R, \theta) \to 0$. Evidently the drag on at-

tached floc particles is associated with u_θ. The viscous drag (which generates the tangential stress driving our "squeeze-out" mechanism) is given by

$$df_v = \eta \left.\frac{\partial u_\theta}{\partial r}\right|_{r=R} dA \tag{46}$$

where dA is the element of area on which the drag is exerted.

Schlichting (26) gives plots of

$$u_\theta(\theta, y)/U_\theta(\theta, y) \equiv f(\theta, y) \tag{47}$$

as a function of

$$Y = \left(\frac{u_\infty R\rho}{\eta}\right)^{1/2} \frac{y}{R}, \qquad y = r - R \tag{48}$$

for various values of θ between 0° and 109.6°, at which point boundary layer separation occurs.

So

$$u_\theta(\theta, y) = U_\theta(\theta, y) f(\theta, Y) \tag{49}$$

Then

$$\frac{\partial u_\theta}{\partial r} = \frac{\partial u_\theta}{\partial y} = \frac{\partial U_\theta}{\partial y}(\theta, y) f(\theta, Y) + \frac{\partial f}{\partial Y}(\theta, Y) \frac{dY}{dy} U_\theta(\theta, Y) \tag{50}$$

We wish to evaluate this derivative at $r = R$, or $y = Y = 0$. We see from Schlichting's plots that $f(\theta, 0) = 0$, so we obtain

$$\left.\frac{\partial u_\theta}{\partial r}\right|_{r=R} = U_\theta(\theta, 0) \frac{\partial f}{\partial Y}(\theta, 0) \frac{1}{R}\left(\frac{u_\infty R\rho}{\eta}\right)^{1/2} \tag{51}$$

on using Eq. (48). Substituting for U_θ from Eq. (45) and setting $r = R$ yields

$$\left.\frac{\partial u_\theta}{\partial r}\right|_{r=R} = \frac{3}{2}(u_\infty)^{3/2} \left(\frac{\rho}{R\eta}\right)^{1/2} \frac{\partial f}{\partial Y}(\theta, 0) \sin\theta \tag{52}$$

We estimate $\partial f/\partial Y$ from Schlichting's data, as indicated in Table 1. This function is graphed in Fig. 17, in which the function is approximated by a series of lines through points which were obtained from Schlichting's graphs.

We let θ_1 specify the top of the cap of attached particles (see Fig. 16). The tangential surface pressure at $\theta_2 > \theta_1$ is then given by

TABLE 1

Estimation of $\partial f/\partial Y$

θ	$\partial f/\partial Y(\theta, 0)$
0°	2.45
25	2.24
50	1.99
75	1.60
90	1.08
100	0.62
109.6	0.01

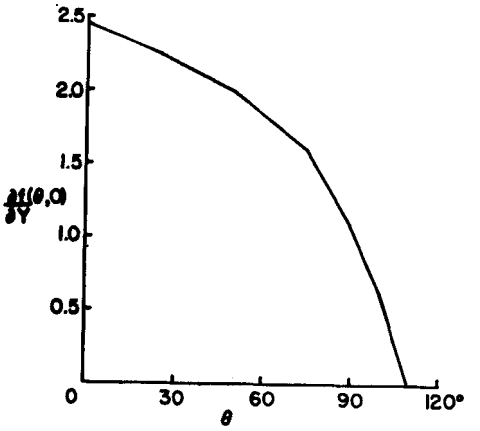

FIG. 17. Plot of $\partial f/\partial Y$ versus θ.

$$P_s(\theta_2, \theta_1) = \int_{\theta_1}^{\theta_2} \eta \left.\frac{\partial u_\theta}{\partial r}\right|_{r=R} R\, d\theta \tag{53}$$

The maximum tangential surface pressure occurs at $\theta_2 = \theta_0 = 109.6°$, at which boundary layer separation occurs. On substituting Eq. (52) into Eq. (53), we obtain for the maximum tangential surface pressure

$$P_s^{\max}(\theta_1) = \frac{3}{2}(u_\infty)^{3/2}(\rho R\eta)^{1/2} \int_{\theta_1}^{\theta_0} \frac{\partial f}{\partial Y}(\theta, 0) \sin\theta\, d\theta \tag{54}$$

We define

$$g(\theta_1) = \int_{\theta_1}^{\theta_0} \frac{\partial f}{\partial Y}(\theta, 0) \sin\theta\, d\theta \tag{55}$$

and evaluate this function by numerical integration of Eq. (55); a plot of $g(\theta_1)$ is shown in Fig. 18.

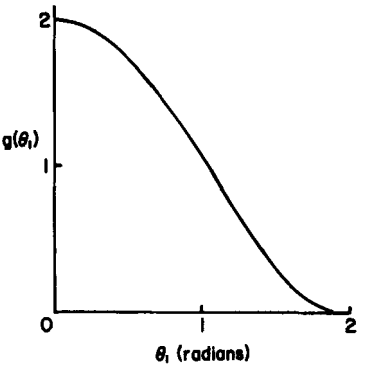

FIG. 18. Plot of $g(\theta_1)$ versus θ_1.

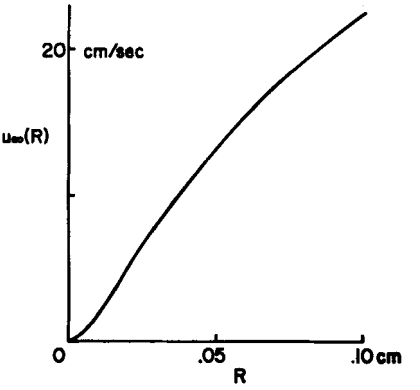

FIG. 19. Bubble rise velocity as a function of bubble radius, from Eq. (40).

We consider floc particles of radius 10^{-5} cm, for which $\Delta G \cong 2 \times 10^{-9}$ erg (*21*). The area occupied by a floc particle on the bubble is about 3.14×10^{-10} cm^2, and the surface pressure required to squeeze out a particle is

$$P_s^1 \simeq \frac{2 \times 10^{-9} \text{ erg}}{3.14 \times 10^{-10} \text{cm}^2} = 6.37 \text{ dyn/cm}$$

Given ρ, R, and η, we can calculate $H(R)$, the factor in front of the integral in Eq. (54); first one must calculate $u_\infty(R)$ from Eq. (40). A plot of $u_\infty(R)$ versus R is shown in Fig. 19, and Reynolds number as a function of R is plotted in Fig. 20. A plot of $H(R)$ versus R is given in Fig. 21. These calculations are for water at 25°C ($\rho = 0.997044$ g/cm^3, $\eta = 0.008937$ poise). For bubbles of radius >0.01 cm, we are evidently out of the creeping flow regime (Re > 1), so our use of inviscid flow streamlines and

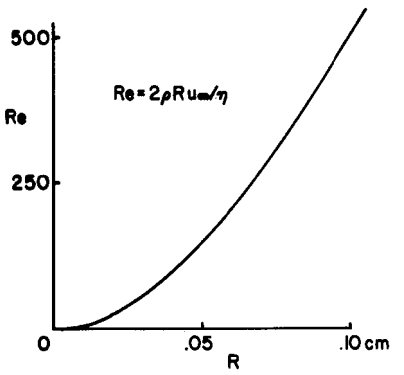

FIG. 20. Reynolds number as a function of bubble radius.

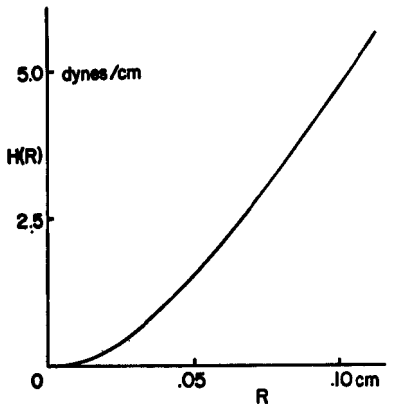

FIG. 21. The preintegral factor $H(R)$ as a function of bubble radius.

boundary layer theory is warranted. For specified values of ρ, R, and η we calculate $H(R)$ and then from Fig. 21 we determine the value of θ_1 which makes $P_s^{\max}(\theta_1) = P_s^1$. This permits us to determine the area of the bubble which may be covered with floc. If we take $P_s' = 6.37$ dyn/cm and assume a bubble radius of 0.05 cm, we find from Fig. 21 that $H(R) =$ 1.50 dyn/cm, so that $g(\theta_1)$ must be less than $6.37/1.50 = 4.25$. We see from Fig. 18 that the maximum value of $g(\theta_1)$ is about 2, so this bubble can be completely coated. A bubble of radius 0.09 cm has $H(R) = 4.02$, so $g(\theta_1)$ must be $\leq 6.37/4.02 = 1.58$. We see from Fig. 18 that θ_1 must be 0.63 radians, from which we find that a fraction

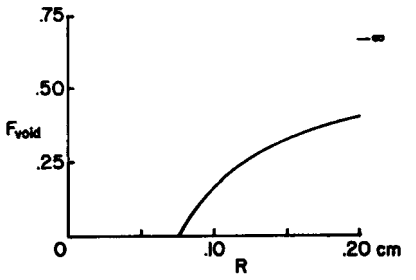

FIG. 22. Void fraction of bubble surface as a function of bubble radius.

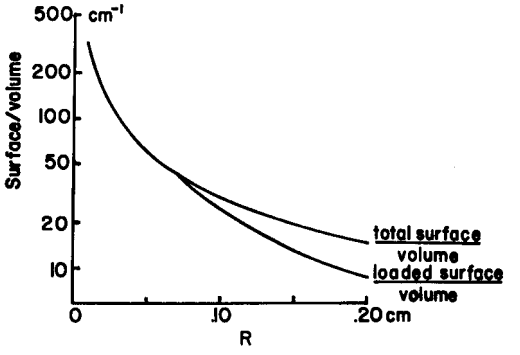

FIG. 23. Total surface/volume and loaded surface/volume ratios as functions of bubble radius.

$$F_{\text{void}} = \frac{\int_0^{2\pi}\int_0^{.63} \sin\theta \, d\theta \, d\phi}{4\pi} = \frac{1 - \cos 0.63}{2} = 0.096$$

of the bubble surface cannot be covered. A plot of the fraction of bubble surface which cannot be covered,

$$F_{\text{void}} = \frac{1 - \cos\theta_1}{2} \tag{56}$$

as a function of R is shown in Fig. 22.

The loaded surface per unit volume of air is given by

$$\frac{S}{V} = \frac{3(1 - F_{\text{void}})}{R} \tag{57}$$

This quantity is plotted (on a semilog scale) as a function of R in Fig. 23.

We see that the removal efficiency decreases markedly due to the squeeze-out mechanism for $R > 0.0775$ cm, although the drop-off is not as extreme as was calculated in our earlier, simpler model. Bubbles of radius >0.015 cm certainly are out of the creeping flow regime (see Fig. 20), which is desirable (*25*), and bubbles of radius $<.07$ cm can be completely covered with floc. This bubble size range should be optimal for the floc we have selected, and similar analyses can be carried out with these plots for other flocs.

Acknowledgments

This work was supported by a grant from the Vanderbilt University Research Council. J. E. Kiefer was supported by a Harold Stirling Vanderbilt Fellowship.

REFERENCES

1. R. Lemlich (ed.), *Adsorptive Bubble Separation Techniques*, Academic, New York, 1972.
2. P. Somasundaran, *Sep. Sci.*, *10*, 93 (1975).
3. R. B. Grieves, *Chem. Eng. J.*, *9*, 93 (1975).
4. A. N. Clarke and D. J. Wilson, *Sep. Purif. Methods*, *7*, 55 (1978).
5. I. H. Newson, *J. Appl. Chem.*, *16*, 43 (1966).
6. P. A. Haas and H. F. Johnson, *AIChE J.*, *11*, 319 (1965).
7. M. Goldberg and E. Rubin, *Sep. Sci.*, *7*, 51 (1972).
8. L. K. Wang, M. L. Granstrom, and B. T. Kown, *Environ. Lett.*, *3*, 251 (1972).
9. K. D. Cannon and R. Lemlich, *Chem. Eng. Prog. Symp. Ser.*, *68*(124), 180 (1972).
10. S. J. Lee, PhD Dissertation, University of Tennessee, 1969.
11. S. Fanlo and R. Lemlich, Proc. AIChE-Inst. Chem. Eng. Joint Meeting, London, *9*, 75 (1965).
12. R. B. Grieves, I. U. Ogbu, D. Bhattacharyya, and W. L. Conger, *Sep. Sci.*, *5* 583 (1970).
13. E. Valdes-Krieg, C. J. King, and H. H. Sephton, *Sep. Purif. Methods*, *6*, 221 (1977).
14. K. V. Sastry and D. W. Fuerstenau, *Trans. AIME*, *247*, 46 (1970).
15. J. W. Wilson, D. J. Wilson, and J. H. Clarke, *Sep. Sci.*, *11*, 223 (1976).
16. Ref. *1*, Chap. 2.
17. J. A. Dean (ed.), *Lange's Handbook of Chemistry*, 11th ed., McGraw-Hill, New York, 1973, p. 1-73.
18. Ref. *1*, p. 46.
19. S.-d. Huang and D. J. Wilson, *Sep. Sci.*, *10*, 407 (1975).
20. R. M. Kennedy and D. J. Wilson, *Sep. Sci. Technol.*, *15*, 1339 (1980).
21. D. J. Wilson, *Ibid.*, *13*, 107 (1978).
22. B. L. Currin, F. J. Potter, D. J. Wilson, and R. H. French, *Ibid.*, *13*, 285 (1978).
23. R. H. French and D. J. Wilson, *Ibid.*, *15*, 123 (1980).
24. J. E. Kiefer and D. J. Wilson, *Ibid.*, *15*, 57 (1980).
25. R. M. Kennedy and D. J. Wilson, *Ibid.*
26. H. Schlichting, *Boundary Layer Theory*, 7th ed. (trans. by J. Kestin), McGraw-Hill, New York, 1979, p. 238.

27. G. M. Fair, J. C. Geyer, and D. A. Okun, *Water and Wastewater Engineering, Vol. II, Wastewater Treatment and Disposal*, Wiley, New York, 1968, Section 25–2.
28. R. B. Bird, W. E. Stewart, and E. N. Lightfoot, *Transport Phenomena*, Wiley, New York, 1960, p. 149.

Received by editor July 30, 1980